Aerosol and Air Quality Research

ORIGINAL RESEARCH
https://doi.org/10.4209/aaqr.230116

Chemical Composition and Mixing State of Fine Particles during Haze Periods in Yinchuan

Kangning Li [1*], Yanqiu Ma [1], Liukun Li [1], Bin Huang [2]

[1] Ningxia Key Laboratory of Intelligent Sensing for the Desert Information, School of Physics, Ningxia University, Yinchuan 750021, China
[2] Enviromental Monitoring Site of Ningxia Ningdong Energy and Chemical Industry Base, Yinchuan 754100, China

ABSTRACT

In this study, we explored the chemical composition and mixing state of fine atmospheric particles in Yinchuan between December 21 and 31, 2021. For this, the single-particle aerosol mass spectrometry (SPAMS) technique was used. Black carbon particles were found to be the predominant aerosol type (in terms of number fraction) throughout the sampling period, accounting for 61.15% of all sampled particles. Considerable changes were noted in the mixing state of the fine particles in the study area. Furthermore, prominent mass spectrum characteristics of potassium particles were observed. The $^{39}K^+$ signal in the positive mass spectrum was stronger than the other signals. Throughout the sampling process, K-rich and potassium-elemental carbon (KEC) particles accounted for 25.86% and 13.05% of all sampled particles, respectively, followed by OC and NaKEC, which accounted for 12.32% and 11.45%, respectively. With time, complex processes of aerosol concentration variation detected by SPAMS were observed. The number fractions of elemental carbon/organic carbon (ECOC) and KEC particles were significantly higher on polluted days than on clean days. ECOC and KEC particles were more mixed with sulfate and nitrate than EC and NaKEC particles. Compared with clean days, the particle size of each BC particle increased on polluted days. Furthermore, ECOC and KEC particles had larger particle sizes and stronger sulfate and nitrate signals than EC and NaKEC particles, which indicates that ECOC and KEC particles were mostly formed during the aging process. Local pollution events were associated with primary combustion emission and secondary particle generation.

Keywords: Single particle, Mixing state, Chemical composition, Fine particle

Received: May 24, 2023
Revised: August 8, 2023
Accepted: August 8, 2023

* **Corresponding Author:**
knli@nxu.edu.cn

Publisher:
Taiwan Association for Aerosol Research
ISSN: 1680-8584 print
ISSN: 2071-1409 online

1 INTRODUCTION

Aerosol particles are crucial components of the earth's atmosphere. These particles directly or indirectly affect the climate system through radiative forcing (IPCC, 2001). Because of their optical and adverse effects on the living environment and human health, aerosol particles have been paid considerable attention (Li *et al.*, 2017; Li *et al.*, 2018; Yang *et al.*, 2011). Concentration and particle size are two key parameters of aerosols; various methods are used to evaluate these parameters. With the frequent occurrence of pollution events, air pollution has become a severe problem in Yinchuan. Therefore, the chemical composition of $PM_{2.5}$ in polluted cities should be investigated. Gaining an in-depth understanding of the chemical and source composition of $PM_{2.5}$ may help us elucidate the mechanisms of air pollution. Most studies on the chemical composition and source of $PM_{2.5}$ have relied on offline measurements. However, offline sampling is time-consuming and yields low-resolution data and thus cannot be used to evaluate the rapid response to short-term and frequent pollution events. To overcome these shortcomings, high time-resolution instruments, which monitor the chemical composition of aerosols in real-time, have been widely used in $PM_{2.5}$ research in recent years. In this context, single-particle aerosol mass spectrometry (SPAMS) has emerged as a popular technique because it facilitates real-time $PM_{2.5}$ source identification (Luo *et al.*, 2019;

Li *et al.*, 2011; Mu *et al.*, 2013; Zhou *et al.*, 2015; Wen *et al.*, 2018; Peng *et al.*, 2019; Wang *et al.*, 2018; Zhang *et al.*, 2023) and determines both particle size and chemical composition at the single-particle level (Li *et al.*, 2018; Li *et al.*, 2011; Wen *et al.*, 2018; Zhou *et al.*, 2023; Chen *et al.*, 2024). Particle concentration can reflect, to some extent, the status of fine particle pollution in the atmosphere (Yu *et al.*, 2019). Numerous studies have been conducted across China, for example in Shanghai (Mu *et al.*, 2013; Yang *et al.*, 2012; Li *et al.*, 2021), Beijing (Ma *et al.*, 2016), Guangzhou (Zhang *et al.*, 2015; Bi *et al.*, 2016; Zhang *et al.*, 2013; Yun *et al.*, 2024; Zhou *et al.*, 2020), and Chongqing (Chen *et al.*, 2017), to determine the size and chemical composition of local atmospheric particles and comprehensively investigate the source and mixing state of individual particles.

Sun *et al.* (2023) studied the single-particle volatility in winter in Beijing by a thermodenuder coupled with SPAMS and the results shown that organic nitrogen-containing particles dominated the total low-volatility particles. Using SPAMS, single-particle chemical composition, volatility and mixing state measurements of urban aerosol particles in Chengdu was investigated, and the results shown that photochemical reaction plays an important role in the formation of KSO_4 particles (Sun *et al.*, 2023). Zhang *et al.* (2017b) explored the chemical composition of individual particles in Sichuan Basin during summer; they found that biomass combustion and industrial emission substantially contributed to $PM_{2.5}$ pollution in Chengdu. Wang *et al.* (2015) investigated the mixing state of carbon-containing aerosols during the Nanjing haze event and found that the degree of carbon aerosol and secondary component mixing increased on haze days. Ma *et al.* (2019) evaluated the chemical composition and mixing state of particles during an autumn haze event in Beijing; they indicated the crucial contribution of secondary aerosol generation to haze formation. Zhang *et al.* (2017a) studied the mixing state of particles in haze weather in Zhengzhou; they observed an increased degree of particle and secondary component mixing during the haze event and the severe aging of particles. He *et al.* (2013) observed considerable increases in particle size and secondary component generation in haze weather; they further reported that the haze process was caused mainly by the aging of elemental carbon (EC), EC/organic carbon (ECOC), and potassium-rich (K-rich) particles and the concentrated burning of rice straw. Yan *et al.* (2019) used SPAMS to investigate the effects of air mass movement on the changes in marine atmospheric aerosols. Luo *et al.* (2019) analyzed the single-particle characteristics of aerosols in Chengdu during a pollution event in winter; they reported that local combustion was primarily responsible for light pollution and both local combustion and long-distance transport contributed to heavy pollution. The mixing of sulfate and nitrate markedly increased with the worsening of air quality. Bi *et al.* (2011) reported that the nitrogen content in aerosol particles originating from biomass combustion was 10% higher than that in aerosol particles from other sources. Shen *et al.* (2020) investigated the mixing state and spectral distribution of aerosols transported by dust over a long distance; they showed that the peak value of the spectral distribution of most aerosol particles during the dust period was 0.66 μm, which was 0.12 μm higher than that observed during a nondust period. Zhang *et al.* (2019) demonstrated that the contributions of combustion-generated particles and aging organic carbon (OC) particles to the formation of rich amine solution were relatively high in summer and winter, respectively.

Yinchuan City is located in northwest China. The annual average $PM_{2.5}$ concentration in this city generally exhibits a downward trend; however, regional $PM_{2.5}$ pollution increases in winter. Recently, Yinchuan experienced severe air pollution, including $PM_{2.5}$ and gaseous pollution (Li *et al.*, 2022a; Zou *et al.*, 2018). The physicochemical properties of atmospheric aerosols in Yinchuan considerably change because of the local emission of pollutants and the long-distance transport of pollutants from other heavily polluted areas (Li *et al.*, 2022a).

In this study, we investigated the characteristics, composition, and sources of fine particles in Yinchuan. SPAMS was used to perform a real-time online source analysis of the main components of $PM_{2.5}$ and evaluate the effects of various pollution sources on $PM_{2.5}$. Using meteorological data, we analyzed the time variation in the pollution sources across Yinchuan to obtain basic data for the analysis of $PM_{2.5}$ pollution sources and provide technical references for the effective formulation of atmospheric environmental protection strategies for Yinchuan.

2 MATERIALS AND METHODS

2.1 SPAMS

SPAMS (Hexin Analytical Instruments, Guangzhou, China) facilitates the online evaluation of the particle size and chemical composition of individual aerosols, thus providing a basis for the assessment of aerosol source and evolution. The instrument can measure particles with diameters ranging from 0.2 to 2.0 μm. The sampling flow rate and ionization energy of the instrument are approximately 0.1 L min^{-1} and 0.6 mJ $pulse^{-1}$ during a normal operation. SPAMS is primarily composed of an air intake system, a diameter measurement system, and a mass spectral detection system (Li *et al.*, 2018; Li *et al.*, 2021; Zhai *et al.*, 2015; Li *et al.*, 2022b; Li *et al.*, 2014).

During analysis, the target aerosol particle first passes through a flow-limiting hole of approximately 100 μm and then enters the aerodynamic lens system. The main function of this system is to focus the aerosol into a particle beam, ensuring that all particles are focused on the same straight line, which facilitates the subsequent determination of particle size and composition. Although almost all aerosols pass through the aerodynamic lens system, information on chemical composition is obtained only for approximately 30% of all particles.

The primary function of the diameter measurement system is to measure the aerodynamic particle size of individual aerosols. When the outside gas enters the mass spectrometer, it rapidly expands under the pressure difference resulting from an internal vacuum of $>$ 2.0 Torr. At this time, the particles carried by the gas are accelerated; the accelerated speed of a particle corresponds to its aerodynamic particle size one by one. SPAMS uses two lasers (wavelength of both lasers, 532 nm) to determine the size of individual particles. The scattered signal of particles passing through the laser beam is converted into an electrical signal by a photomultiplier tube, which is used to mark the moment of particles passing through the laser beam. Through this approach, the time interval between the passages of an aerosol particle through the two laser beams can be evaluated. The ratio of the distance (fixed value) between the two laser beams to the time interval can be used to calculate aerosol velocity and aerodynamic particle size.

The main function of the mass spectral detection system is to provide information on the mass spectrum of aerosols. SPAMS calculates the time when an aerosol reaches the detection system on the basis of the velocity of the aerosol after diameter measurement. When the aerosol enters a specific location in the ionization region, it excites the YAG laser (wavelength, 266 nm). The YAG laser vaporizes the chemical components of the aerosol to form positive and negative ions. These ions are extracted by the electrode and accelerated under the acceleration voltage and subsequently analyzed by a bipolar mass analyzer. Finally, the positive and negative mass spectral data of the aerosol are recorded by a time-of-flight mass spectrometer.

2.2 Aerosol Sampling and Data Analysis

SPAMS was used to conduct the field observations of fine particles in the atmosphere between December 21 and 31, 2021. The sampling site was located in the Linhe Industrial Park of Ningdong Base (106°32′12″E; 38°13′4″N). The monitoring site was surrounded by Hengshan Road and Chaoyang Road (traffic roads), with Ningxia Baofeng Energy Zone to the north, the Ningdong Aluminum Branch of Qingtongxia Aluminum Co., Ltd. to the southwest, and Ningxia Jingneng Ningdong Power Generation Co., Ltd. to the southeast.

Online SPAMS and other instruments were used for continuous sampling and real-time analysis. Meteorological conditions and the atmospheric mass concentrations of nitrogen dioxide and sulfur dioxide were measured synchronously. EC ion clusters are considered to be key markers of black carbon (BC) aerosols (Gong *et al.*, 2016). Using $C_n^{\pm}$ (n = 1, 2, 3...) as the BC marker, we identified 113,382 BC-containing particles, which accounted for approximately 61.15% of all sampled particles. We used the clustering algorithm based on adaptive resonance theory (ART-2a) to process the SPAMS data (Du *et al.*, 2010). After reviewing other studies (Gong *et al.*, 2016; Wang *et al.*, 2016; Jayne *et al.*, 2000; Zhang *et al.*, 2018), we set the alert factor, learning efficiency, and iteration times of the ART-2a algorithm to 0.85, 0.05, and 20, respectively.

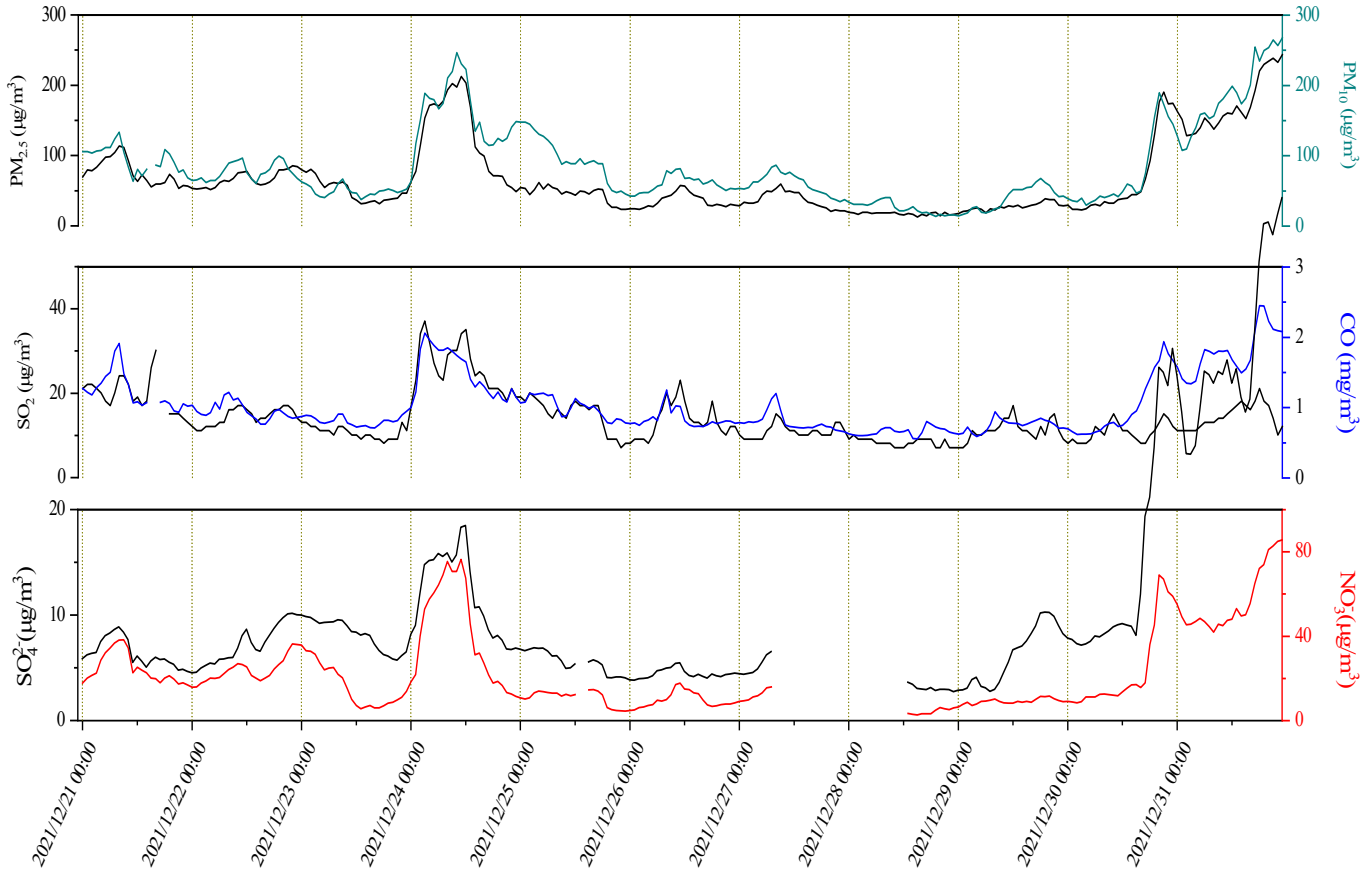

Fig. 1. Temporal profiles of the mass concentrations of $PM_{2.5}$, PM_{10}, sulfur dioxide, carbon monoxide, sulfate, and nitrate.

3 RESULTS AND DISCUSSION

3.1 Air Quality and Meteorological Conditions

Temporal data on the mass concentrations of $PM_{2.5}$, PM_{10}, sulfur dioxide, carbon monoxide, sulfate, and nitrate were provided by the nearby Ningxia Ecological Environment Monitoring Center. The carbon monoxide concentration showed three major peaks: 1.909, 2.057, and 1.936 mg m^{-3} at 08:00 on December 21, at 03:00 on December 24, and at 21:00 on December 30, respectively (Fig. 1). The mass concentration of sulfur dioxide exhibited the same trend as that of carbon monoxide. The mass concentration of $PM_{2.5}$ peaked thrice on December 21, 24, and 30; the maximum value was 220 μg m^{-3} (18:00 local time on December 30). The average mass concentration of $PM_{2.5}$ during the same period was 65.10 μg m^{-3}. The trend of PM_{10} concentration was similar to that of $PM_{2.5}$ concentration, and it varied from 13 to 267 μg m^{-3}, with an average of 83.24 μg m^{-3}.

3.2 Classification and Size Distribution of Ambient Particles

A total of 185,411 particles with positive and negative mass spectra were detected through SPAMS. Using the Art-2a algorithm, we classified all particles into 11 types; these types were named on the basis of the main components present in them. The characteristic components of each particle type were listed in Table 1, and the number and number fraction of each particle type were listed in Table 2. Except "others", the average mass spectral profiles of the 10 particle types were presented in Fig. 2.

The mass spectra of EC particles exhibited carbon cluster peaks $C_n^{\pm}$ (n = 1, 2, 3...). In addition, weak signals of secondary components, such as sulfate and nitrate, were recorded, which indicated that pure EC does not undergo considerable aging in the atmosphere; therefore, EC was regarded as freshly emitted BC particles. ECOC particles predominantly exhibited carbon cluster peaks.

Table 1. Characteristic components of various particles.

Type	The Main Components
EC	$^{12n}C_n^{\pm}$
ECOC	$^{12n}C_n^{\pm}$, $^{29}C_2H_5^+$, $^{37}C_3H^+$, $^{39}C_3H_3^+$, $^{43}CH_3CO^+$
KEC	$^{12n}C_n^{\pm}$, $^{39/41}K^+$, $^{26}CN^-/C_2H_2^-$, $^{35/27}Cl^-$, $^{80}SO_3^-$
NaKEC	$^{12n}C_n^{\pm}$, $^{23}Na^+$, $^{39/41}K^+$, $^{26}CN^-/C_2H_2^-$, $^{35/27}Cl^-$, $^{80}SO_3^-$
KNa	$^{39/41}K^+$, $^{23}Na^+$
Krich	$^{39/41}K^+$, $^{26}CN^-$, $^{42}CNO^-$
OC	$^{27}C_2H_3^+$, $^{29}C_2H_5^+$, $^{37}C_3H^+$, $^{39}C_3H_3^+/K^+$, $^{43}CH_3CO^+$, $^{51}C_4H_3^+$, $^{55}C_4H_7^+$, $^{63}C_5H_3^+$, $^{77}C_6H_5^+$, $^{91}C_7H_7^+$, $^{115}C_9H_7^+$
Dust	$^{24}Mg^+$, $^{27}Al^+$, $^{40}Ca^+$, $^{55}Mn^+$, $^{56}CaO/Fe^+$, $^{96}Ca_2O^+$, $^{112}Ca_2O_2^+$, $^{43}AlO^-$, $^{60}SiO_2^-$, $^{76}SiO_3^-$
Metal	$^{51}V^+$, $^{52}Cr^+$, $^{55}Mn^+$, $^{56}Fe^+$, $^{63/65}Cu^+$, $^{67}VO^+$, $^{72}FeO^+$, $^{73}FeOH^+$, $^{206/207/208}Pb^+$
Seasalt	$^{23}Na^+$, $^{46}Na_2^+$, $^{81}Na_2Cl^+$, $^{35/27}Cl^-$, $^{147}Na(NO_3)_2^-$
Others	In addition to the above 10 types

Table 2. Number and number fraction of each particle type.

Type	Particle number	Number fraction
EC	3115	1.68%
ECOC	16337	8.81%
KEC	24196	13.05%
NaKEC	21233	11.45%
KNa	5941	3.21%
Krich	47951	25.86%
Dust	16868	9.10%
Metal	15954	8.61%
Sea salt	8843	4.77%
OC	22841	12.32%
Others	2114	1.14%
Total Particles	185393	100%

The positive spectrum contained prominent organic matter peaks ($^{37}C_3H^+$ and $^{43}CH_3CO^+$). By contrast, strong signals of sulfate ($^{97}HSO_4^-$) and nitrate ($^{46}HSO_2^-$ and $^{62}NO_3^-$) were observed in the negative spectrum. ECOC particle size was larger than that EC particle, which indicates that ECOC particle originates from EC particle through atmospheric aging (Moffet and Prather 2009; Sullivan *et al.*, 2007). Potassium-EC (KEC) particles are mainly derived from biomass or coal combustion. We observed prominent peaks of $^{39/41}K^+$ and $^{213/215}K_3SO_4^+$ in the positive mass spectrum and those of nitrogen-containing organic compounds ($^{26}CN^-$, $^{26}C_2H_2^-$, and $^{42}CNO^-$) in the negative spectrum. NaKEC particles exhibited a high number of carbon cluster peaks ($C_n^{\pm}$). Prominent $^{23}Na^+$ and $^{39}K^+$ peaks were noted in the positive mass spectrum. These particles may arise from traffic sources (Cheng *et al.*, 2013).

The positive mass spectrum of K-rich particles exhibited a strong potassium ion ($^{39}K^+$) signal but a weak carbon cluster ($C_n^{\pm}$) signal. The peaks of $^{26}CN^-$ and $^{42}CNO^-$ in the negative spectrum were prominent and revealed strong signals for sulfate ($^{97}HSO_4^-$) and nitrate ($^{46}NO_2^-$ and $^{62}NO_3^-$). K-rich particles may be identified as secondarily produced particles (Johnson *et al.*, 2004; Xu *et al.*, 2017). The mass spectrum of OC particles exhibited a high OC concentration. OC is emitted from diverse sources in daily life, such as industrial, catering, and transportation sources (Huo *et al.*, 2016). KNa particles exhibited strong potassium ($^{39}K^+$) and sodium ($^{23}Na^+$) ion signals but weak carbon ion signals. The negative spectrum contained weak $^{16}O^-$, $^{26}CN^-$, and $^{35/37}Cl^-$ signals and strong nitrate and sulfate signals. Sea salt is a common aerosol; it exhibited significant sodium ion ($^{23}Na^+$) and sodium-containing ion clusters ($^{81}Na_2Cl^+$) in the positive mass spectrum and chloride ($^{35/37}Cl^-$) signals in the negative spectrum (Clarke *et al.*, 2007). Metal contained various metal components, such as $^{51}V^+$, $^{55}Mn^+$, $^{56}Fe^+$, and $^{206/207/208}Pb^+$. These particles are emitted primarily from chemical, metallurgical, and other industrial sources (Wang *et al.*, 2016; Saleh *et al.*, 2014). Dust particles contained various crustal elements, such as $^{27}Al^+$ and $^{40}Ca^+$; these particles arise from atmospheric dust (Knudsen *et al.*, 2004; Romero and Oehme 2005).

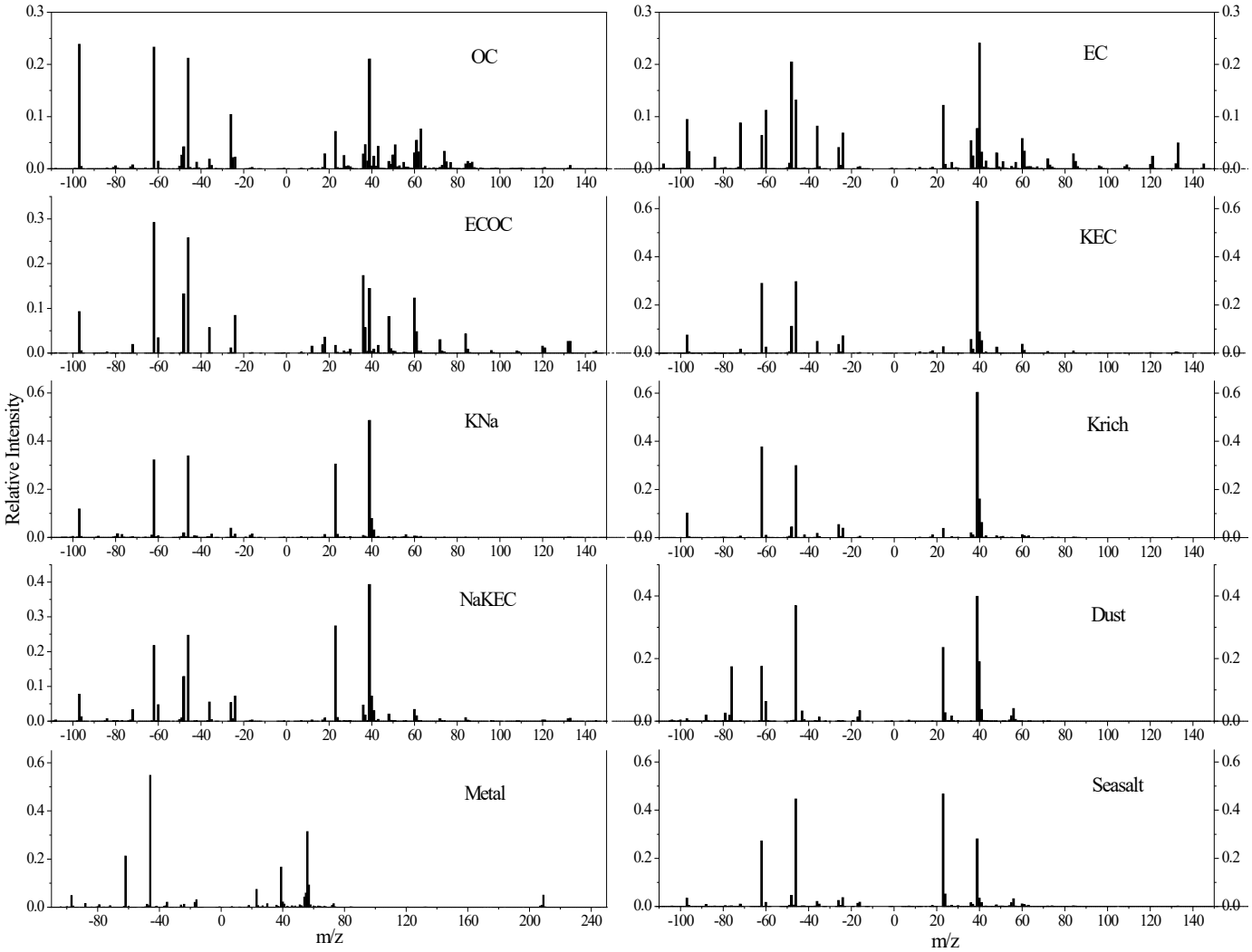

Fig. 2. Average mass spectral profiles of 11 particle types.

Other particles did not belong to any of the top 10 types and accounted for only 1.14% of the total number of particles. Therefore, we did not evaluate these particles in this study.

Fig. 3 shows the size distribution of various particles. The size of the particles detected by SPAMS ranged from 200 to 1200 nm. The particle types varied considerably in terms of number fraction and size. In the range between 200 to 600 nm, EC, NaKEC, and small amounts of ECOC and OC were mainly detected. Particles with a size of > 600 nm primarily included ECOC, KEC, metal, and dust.

3.3 Temporal Variations in Ambient Aerosols

The mass spectrum characteristics of potassium particles were prominent, and the $^{39}K^{+}$ signal in the positive mass spectrum was stronger than the other signals. $^{39}K^{+}$, which arises from the direct emission from biomass combustion, is a tracer of this process (Xu *et al.*, 2017). The pie chart in Fig. 4 shows the number fractions of various particles. Throughout the sampling process, K-rich and KEC particles accounted for 25.86% and 13.05% of all sampled particles, respectively, followed by OC and NaKEC, which accounted for 12.32% and 11.45%, respectively.

To investigate the source of pollutants, we calculated the temporal variation in the number concentrations of the 11 particle types detected using SPAMS (Fig. 5). The number concentrations of the particles rapidly changed with time, and the change pattern was complex. For convenience, we defined the following five periods: Period 1, 0:00 to 12:00 on December 22; Period 2, 12:0:00

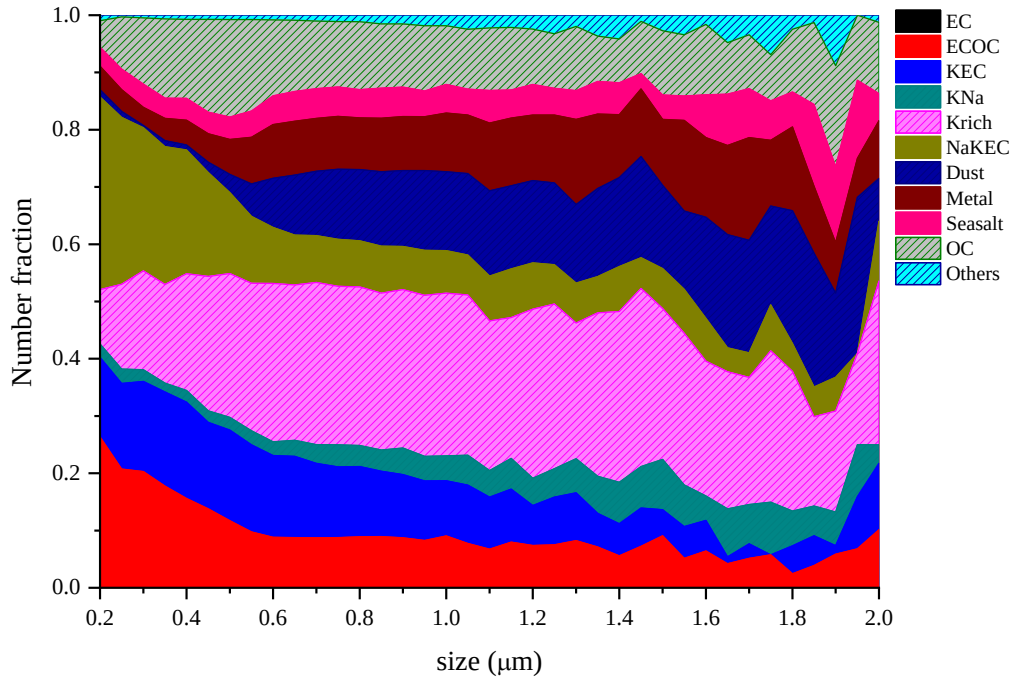

Fig. 3. Size distribution of various particles.

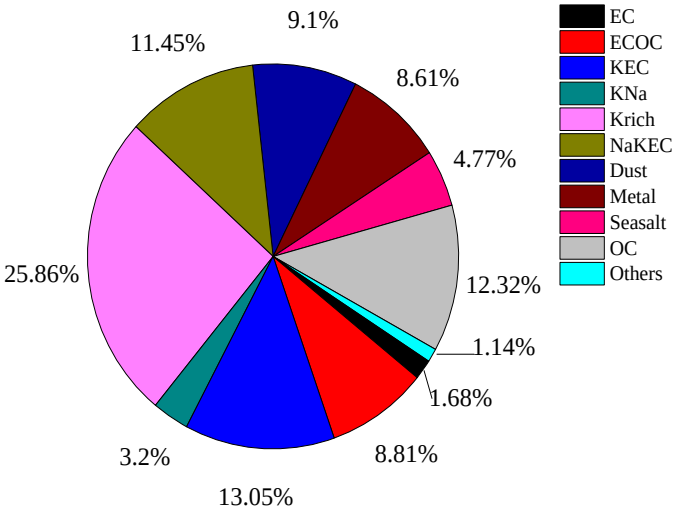

Fig. 4. Number fractions of various particles.

to 24:00 on December 23; Period 3, 0:00 to 24:00 on December 24; Period 4, 0:00 to 24:00 on December 26; and Period 5, 0:00 to 24:00 on December 31.

The average mass concentrations of $PM_{2.5}$ in the Yinchuan urban area were 50.25 and 35.04 μg m^{-3} during Period 2 and Period 4, respectively. The number of particles measured using SPAMS was relatively small. Thus, the days corresponding to these periods were regarded as clean days. The average mass concentrations of $PM_{2.5}$ were 65.88, 126.50, and 172.33 μg m^{-3} during Period 1, Period 3, and Period 5, respectively. The number of particles measured using SPAMS increased significantly. Therefore, the days corresponding to these periods were regarded as polluted days. Period 2 and Period 4 are marked with light green, and Period 1, Period 3, and Period 5 are marked with light yellow. As mentioned, during the observation period, the particles were divided primarily into the following 11 types: EC, ECOC, KEC, KNa, K-rich, NaKEC, dust, metal, sea salt, OC, and other particles.

The pie chart of Fig. 5 represents the number fraction of each particle type in all particles detected by SPAMS at different stages. Among the 11 particles, K-rich particles had the highest number fraction on both clean and polluted days; the value was the lowest during Period 2 (23.5%) and the highest during Period 3 (33.9%). The number fraction of OC particles was 15.5% during Period 3 and Period 4 and only 8.4% during Period 2. The number fraction of KEC particles was the highest (21.2%) during Period 2 and the lowest (9.1%) during Period 4. The number fraction of NaKEC particles exhibited no considerable variation across the periods; this value was approximately 11% during all periods. The number fraction of ECOC particles on clean days during Period 4 was the lowest (3%); however, this value was 13.1% on clean days during Period 2, which is higher than that on polluted days. The number fraction of metal particles on clean days during Period 2 and Period 4 was relatively low (6.8% and 4%, respectively), which is lower than that on polluted days.

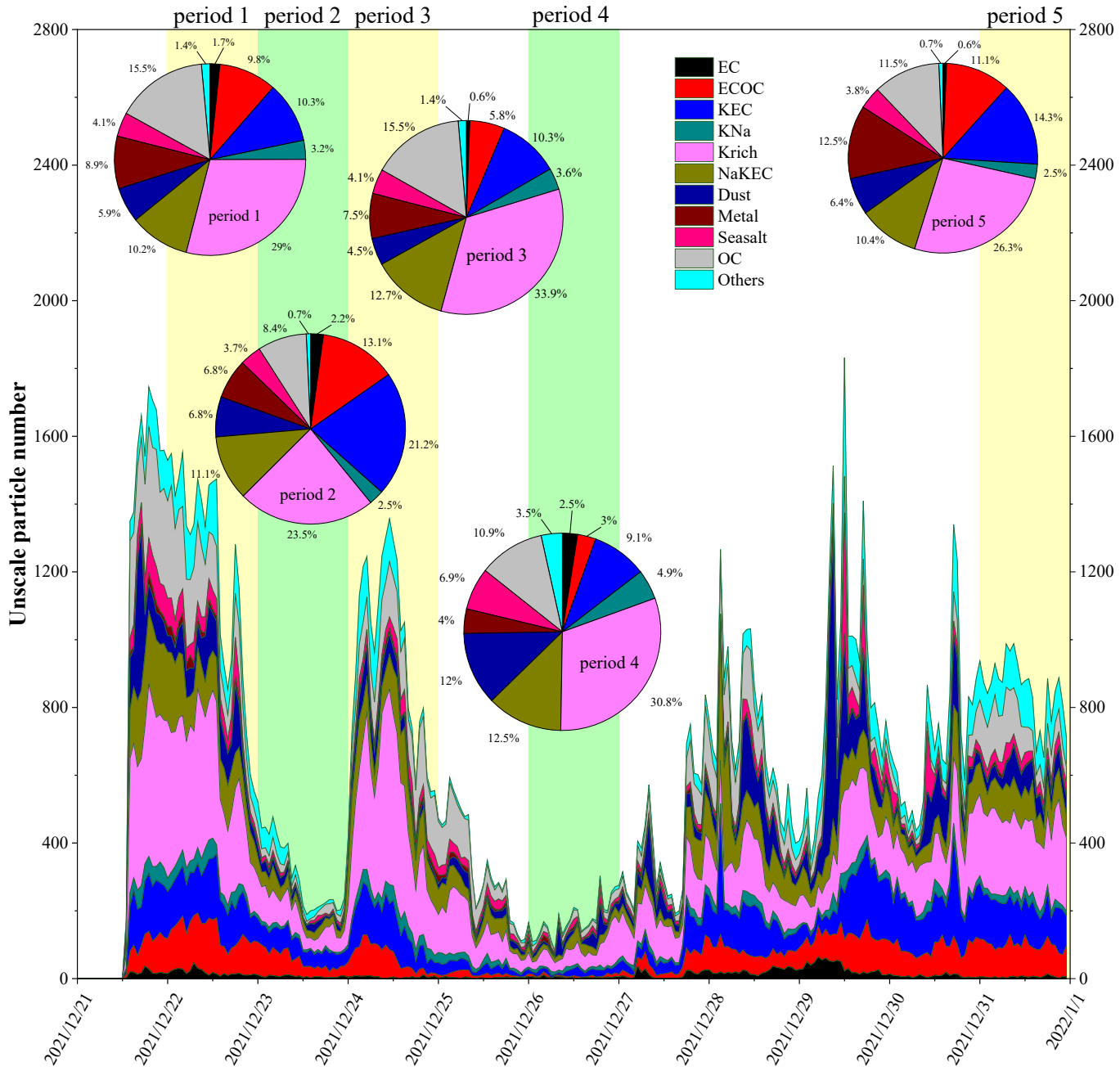

Fig. 5. Temporal variation in the number concentrations of 11 particle types. The pie chart represents the number fraction of each particle type in all particles detected by SPAMS at different stages.

The number fraction of dust particles was the highest (12%) on clean days during Period 4; this value was 6.8% during Period 2 and 6.4% on polluted days. The number fraction of sea salt particles was 6.9% during Period 4, which had the lowest concentration. The number fraction of sea salt remained almost constant across the periods. The number fraction of other particles was 3.5% during Period 4 and < 1.5% during other periods. Furthermore, the number fraction of KNa particles was 4.9% during Period 4 and only 2.5% during Period 2 and Period 5. The number fraction of EC particles was the highest on clean days during Period 2 and 4 (2.2% and 2.35%, respectively). On polluted days, this value was 1.7% during Period 1 and 0.6% during Period 3 and Period 5. Compared with the value obtained on clean days (Period 2 and Period 4), the number fraction of EC particles markedly decreased on pollution days and reached the lowest (0.59%) during Period 3; this value was the highest (2.49%) during Period 4. These findings indicate that most EC particles in the environment underwent aging.

Fig. 6 shows the temporal variation in the number concentration of five BC particle types. The pie chart of Fig. 6 represents the number fraction of each BC type in the total BC particle number at different stages. Among the five types, EC particles had the highest number fraction (4.4%) during Period 4 and the lowest number fraction (0.8%) during Period 3. The number fraction of KEC particles was the highest, and its number fraction was almost constant across the five periods; the highest value was 55.3% during Period 3, and the lowest value was 52.5% during Period 1. The number fraction of NaKEC was the highest (20.6%) during Period 4; during Period 2, the number fraction of NaKEC was the lowest (14.3%). The number fraction of NaKEC did not vary considerably across the polluted days (3.1%). The number fraction of ECOC particles during Period 1, Period 3 and Period 5 was only 0.7%, 7%, and 7.7% higher than that during Period 3, respectively. By contrast, the number fraction of ECOC particles during Period 2 and Period 4 was 22.1% and 5.9%, respectively. The number fraction of other particles was < 7% during Period 2 but > 10% during other periods; the highest value was 15.6% during Period 4, and the lowest value was 11.5% during Period 1.

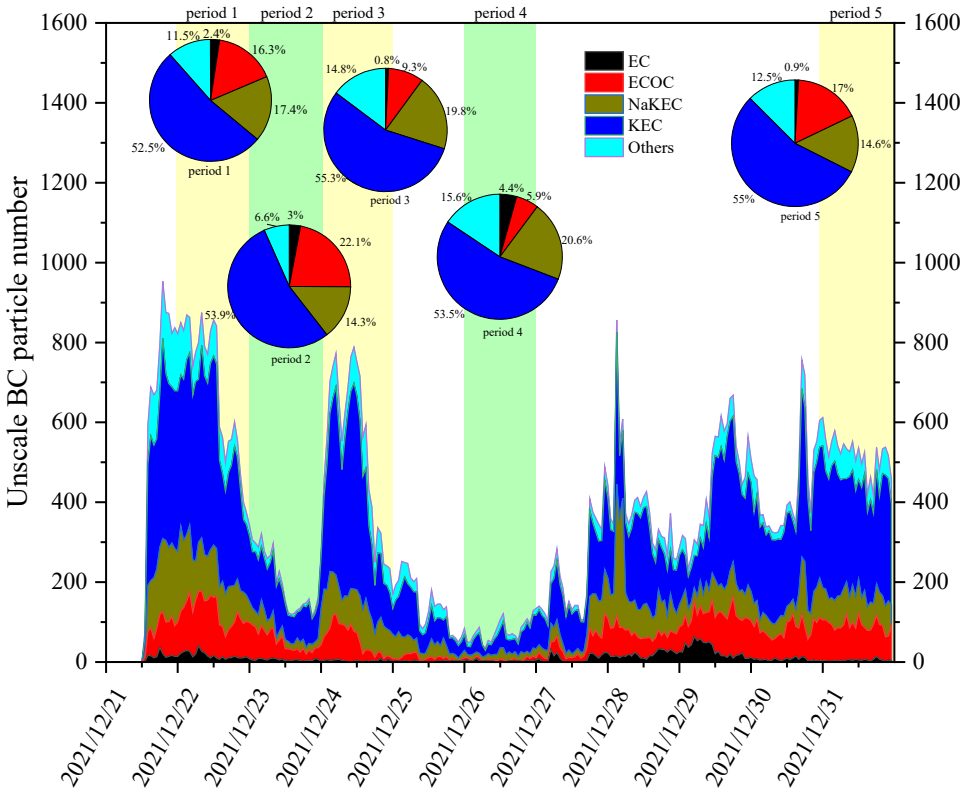

Fig. 6. Temporal variation in the number concentrations of five black carbon particle types. The pie chart represents the number fraction of each BC type in the total BC particle at different stages.

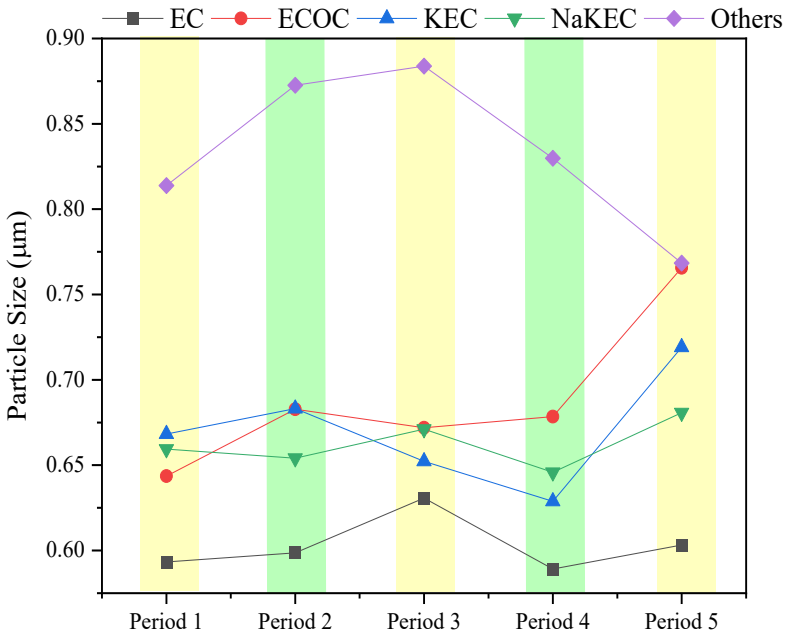

Fig. 7. The size distributions of different BC particles at different periods.

The chemical composition of the particles substantially varied across pollution stages. The number fractions of ECOC and KEC particles increased significantly on polluted days compared with their number fractions on clean days. ECOC and KEC particles had larger particle sizes and exhibited stronger sulfate and nitrate signals than did EC and NaKEC particles; this finding indicates that ECOC and KEC particles are mostly formed after the aging process. The analysis of secondary inorganic ions (Fig. 1) revealed that the degree of mixing of nitrate and sulfate with other particle types was higher on polluted days than on clean days, which is consistent with the findings of other studies (Moffet and Prather, 2009; Giorio *et al.*, 2015). This finding indicates an increased degree of particle aging during pollution. The primary causes of pollution were identified to be anthropogenic emission and secondary particle generation.

Fig. 7 shows the size distributions of different BC particles at different periods. It is obvious from the figure that the particle size of EC, NaKEC and ECOC on polluted days is larger than that on clean days. Their particle size reaches its maximum value at Period 5, which is consistent with the trend of $PM_{2.5}$ mass concentration, while the size of "Others" particle reaches the minimum value at Period 5, which may be related to the small number of particles. Compared with clean days, the particle size of each BC particle increased on polluted days. The size distributions of different type particles at different periods indicate that the deterioration of air quality contributes to the particle size.

4 CONCLUSIONS

Using SPAMS, we analyzed the main components of atmospheric $PM_{2.5}$ in Yinchuan between December 21 and 31, 2021. During the monitoring period, 167,000 particles with both particle size and positive and negative spectrum data were identified in monitoring sites. Using the ART-2a neural network algorithm, we classified fine ambient particles into 11 types according to their mass spectral patterns. The size distribution and the temporal variation in the chemical composition of each particle type were analyzed. The size of the particles ranged from 200 to 1200 nm. The particle types varied substantially in terms of number fraction and size. In the size range between 200 and 600 nm, EC, NaKEC, and small amounts of ECOC and OC were mainly noted; particles with a size of $>$ 600 nm primarily included ECOC, KEC, metal, and dust. The particles' number concentrations over time indicated that the number fractions of ECOC and KEC particles increased most significantly during the pollution period; furthermore, the degree of mixing of ECOC and

KEC particles with sulfate and nitrate was higher than that of mixing EC and NaKEC particles with sulfate and nitrate. These findings indicate that anthropogenic emission and secondary particle generation are the primary causes of pollution. During the pollution period in the study area, wind speed was low and humidity was high; these weather conditions are conducive to the accumulation and secondary generation of pollutants.

DATA AVAILABILITY STATEMENT

The original contributions presented in the study are included in the article/supplementary material, further inquiries can be directed to the corresponding author.

ACKNOWLEDGMENTS

This work was supported by the National Natural Science Foundation of China, grant number 42167016. The Natural Science Foundation of Ningxia Province in China, grant number 2022AAC03123. The Key Research and Development Program of Ningxia Province in China, grant number 2020BEB04003, and the fifth batch of the Ningxia Youth Science and Technology Talents Project, grant number NXTJGC147.

REFERENCES

Bi, X., Zhang, G., Li, L., Wang, X., Li, M., Sheng, G., Fu, J., Zhou, Z. (2011). Mixing state of biomass burning particles by single particle aerosol mass spectrometer in the urban area of PRD, China. Atmos. Environ. 45, 3447–3453. https://doi.org/10.1016/j.atmosenv.2011.03.034

Bi, X., Lin, Q., Peng, L., Zhang, G., Wang, X., Brechtel, F.J., Chen, D., Li, M., Peng, P., Sheng, G., Zhou, Z. (2016). In situ detection of the chemistry of individual fog droplet residues in the Pearl River Delta region, China. J. Geophys. Res. 121, 9105–9116. https://doi.org/10.1002/2016JD024886

Chen, L., Zhang, J., Li, J., Huang, X., Xiang, Y., Chen, J., Pan, T., Zhang, W. (2024). Real-time, single-particle chemical composition, volatility and mixing state measurements of urban aerosol particles in southwest China. J. Environ. Sci. 136, 361–371. https://doi.org/10.1016/j.jes.2022.12.014

Chen, Y., Wenger, J.C., Yang, F., Cao, J., Huang, R., Shi, G., Zhang, S., Tian, M., Wang, H. (2017). Source characterization of urban particles from meat smoking activities in Chongqing, China using single particle aerosol mass spectrometry. Environ. Pollut. 228, 92–101. https://doi.org/10.1016/j.envpol.2017.05.022

Cheng, Z., Wang, S., Jiang, J., Fu, Q., Chen, C., Xu, B., Yu, J., Fu, X., Hao, J. (2013). Long-term trend of haze pollution and impact of particulate matter in the Yangtze River Delta, China. Environ. Pollut. 182, 101–110. https://doi.org/10.1016/j.envpol.2013.06.043

Clarke, A., McNaughton, C., Kapustin, V., Shinozuka, Y., Howell, S., Dibb, J., Zhou, J., Anderson, B., Brekhovskikh, V., Turner, H., Pinkerton, M. (2007). Biomass burning and pollution aerosol over North America: Organic components and their influence on spectral optical properties and humidification response. J. Geophys. Res. 112, D12. https://doi.org/10.1029/2006JD007777

Du, H., Kong, L., Cheng, T., Chen, J., Yang, X., Zhang, R., Han, Z., Yan, Z., Ma, Y. (2010). Insights into ammonium particle-to-gas conversion: non-sulfate ammonium coupling with nitrate and chloride. Aerosol Air Qual. Res. 10, 589–595. https://doi.org/10.4209/aaqr.2010.04.0034

Giorio, C., Tapparo, A., Dall'Osto, M., Beddows, D.C., Esser-Gietl, J.K., Healy, R.M., Harrison, R.M. (2015). Local and regional components of aerosol in a heavily trafficked street canyon in central London derived from PMF and cluster analysis of single-particle ATOFMS spectra. Environ. Sci. Technol. 49, 3330–3340. https://doi.org/10.1021/es506249z

Gong, X., Zhang, C., Chen, H., Nizkorodov, S.A., Chen, J., Yang, X. (2016). Size distribution and mixing state of black carbon particles during a heavy air pollution episode in Shanghai. Atmos. Chem. Phys. 16, 5399–5411. https://doi.org/10.5194/acp-16-5399-2016

He, J., Zhang, G., Wang, B., Chen, D., Bi, X., Zhong, L., Sheng, G., Fu, J., Zhou, Z., Li, L. (2013).

Analysis of single particle characteristics during haze events in Heshan. Acta Sci. Circumst. 33, 2098–2104. https://doi.org/10.13671/j.hjkxxb.2013.08.013 (in Chinese)

Huo, J., Lu, X., Wang, X., Chen, H., Ye, X., Gao, S., Gross, D.S., Chen, J., Yang, X. (2016). Online single particle analysis of chemical composition and mixing state of crop straw burning particles: from laboratory study to field measurement. Front. Environ. Sci. Eng. 10, 244–252. https://doi.org/10.1007/s11783-015-0768-z

Intergovernmental Panel on Climate Change (IPCC) (2001). Climate Change 2001: The Scientific Basis. Contribution of Working Group I to the Third Assessment Report of the Intergovernmental Panel on Climate Change, Houghton, J.T., Ding, Y., Griggs, D.J., Noguer, M., van der Linden, P.J., Dai, X., Maskell, K., Johnson, C.A. (Eds.). Cambridge University Press, Cambridge, United Kingdom and New York, NY, USA, 881pp. https://www.ipcc.ch/site/assets/uploads/2018/03/WGI_TAR_full_report.pdf

Jayne, J.T., Leard, D.C., Zhang, X., Davidovits, P., Smith, K.A., Kolb, C.E., Worsnop, D.R. (2000). Development of an aerosol mass spectrometer for size and composition analysis of submicron particles. Aerosol Sci. Technol. 33, 49–70. https://doi.org/10.1080/027868200410840

Johnson, G., Ristovski, Z., Morawska, L. (2004). Application of the VH-TDMA technique to coastal ambient aerosols. Geophys. Res. Lett. 31, L16105. https://doi.org/10.1029/2004GL020126

Knudsen, J.N., Jensen, P.A., Dam-Johansen, K. (2004). Transformation and release to the gas phase of Cl, K, and S during combustion of annual biomass. Energy Fuels 18, 1385–1399. https://doi.org/10.1021/ef049944q

Li, K., Ye, X., Pang, H., Lu, X., Chen, H., Wang, X., Yang, X., Chen, J., Chen, Y. (2018). Temporal variations in the hygroscopicity and mixing state of black carbon aerosols in a polluted megacity area. Atmos. Chem. Phys. 18, 15201–15218. https://doi.org/10.5194/acp-18-15201-2018

Li, K., Wang, X., Lu, X., Chen, H., Yang, X. (2021). Effect of pollution level on size distributions and mixing state of ambient black carbon particles in an urban area during wintertime. Aerosol Air Qual. Res. 21, 200655. https://doi.org/10.4209/aaqr.200655

Li, K., Li, L., Huang, B., Han, Z. (2022a). Source apportionment of ambient aerosols during a winter pollution episode in Yinchuan by using single-particle mass spectrometry. Atmosphere 13, 1174. https://doi.org/10.3390/atmos13081174

Li, K., Wang, X., Lu, X., Chen, H., Yang, X. (2022b). Effects of volatile components on mixing state and size distribution of individual black carbon aerosols. Aerosol Air Qual. Res. 22, 210400. https://doi.org/10.4209/aaqr.210400

Li, L., Huang, Z., Dong, J., Li, M., Gao, W., Nian, H., Fu, Z., Zhang, G., Bi, X., Cheng, P. (2011). Real time bipolar time-of-flight mass spectrometer for analyzing single aerosol particles. Int. J. Mass Spectrom. 303, 118–124. https://doi.org/10.1016/j.ijms.2011.01.017

Li, L., Li, M., Huang, Z., Gao, W., Nian, H., Fu, Z., Gao, J., Chai, F., Zhou, Z. (2014). Ambient particle characterization by single particle aerosol mass spectrometry in an urban area of Beijing. Atmos. Environ. 94, 323–331. https://doi.org/10.1016/j.atmosenv.2014.03.048

Li, Y.J., Sun, Y., Zhang, Q., Li, X., Li, M., Zhou, Z., Chan, C.K. (2017). Real-time chemical characterization of atmospheric particulate matter in China: A review. Atmos. Environ. 158, 270–304. https://doi.org/10.1016/j.atmosenv.2017.02.027

Luo, J., Huang, X., Zhang, J., Luo, B., Zhang, W., Song, H. (2019). Characterization of aerosol particles during the most polluted season (winter) in urban Chengdu (China) by single-particle analysis. Environ. Sci. Pollut. Res. 26, 17685–17695. https://doi.org/10.1007/s11356-019-05156-4

Ma, L., Li, M., Zhang, H., Li, L., Huang, Z., Gao, W., Chen, D., Fu, Z., Nian, H., Zou, L. (2016). Comparative analysis of chemical composition and sources of aerosol particles in urban Beijing during clear, hazy, and dusty days using single particle aerosol mass spectrometry. J. Cleaner Prod. 112, 1319–1329. https://doi.org/10.1016/j.jclepro.2015.04.054

Ma, Q.K., Cheng, C.L., Li, M., Huang, Z.Z., Gui, H.Q., Zhang, J.S., Zhou, Z. (2019). Chemical composition and mixing state of single particles during the haze period at a Beijing suburb site. Geochimica 48, 195–203. https://doi.org/10.19700/j.0379-1726.2019.02.009

Moffet, R.C., Prather, K.A. (2009). In-situ measurements of the mixing state and optical properties of soot with implications for radiative forcing estimates. Proc. Natl. Acad. Sci. U.S.A. 106, 11872–11877. https://doi.org/10.1073/pnas.0900040106

Mu, Y.Y., Lou, S.R., Chen, C.H., Zhou, M., Wang, H.L., Zhou, Z., Qiao, L.P., Huang, C., Li, M., Li, L.

(2013). Aging and mixing state of particulate matter during aerosol pollution episode in autumn Shanghai using a single particle aerosol mass spectrometer (SPAMS). Environ. Sci. 34, 2071–2080. (in Chinese)

Peng, X., Liu, X., Shi, X., Shi, G., Li, M., Liu, J., Huangfu, Y., Xu, H., Ma, R., Wang, W. (2019). Source apportionment using receptor model based on aerosol mass spectra and 1 h resolution chemical dataset in Tianjin, China. Atmos. Environ. 198, 387–397. https://doi.org/10.1016/j.atmosenv.2018.11.018

Romero, F., Oehme, M. (2005). Organosulfates-A new component of humic-like substances in atmospheric aerosols? J. Atmos. Chem. 52, 283–294. https://doi.org/10.1007/s10874-005-0594-y

Saleh, R., Robinson, E.S., Tkacik, D.S., Ahern, A.T., Liu, S., Aiken, A.C., Sullivan, R.C., Presto, A.A., Dubey, M.K., Yokelson, R.J. (2014). Brownness of organics in aerosols from biomass burning linked to their black carbon content. Nat. Geosci. 7, 647–650. https://doi.org/10.1038/ngeo2220

Shen, L., Hao, F., Gao, M., Wang, H., Zhu, B., Gao, J., Cheng, Y., Xie, F. (2020). Real-time geochemistry of urban aerosol during a heavy dust episode by single-particle aerosol mass spectrometer: Spatio-temporal variability, mixing state and spectral distribution. Particuology 53, 197–207. https://doi.org/10.1016/j.partic.2020.02.001

Sullivan, R., Guazzotti, S., Sodeman, D., Prather, K. (2007). Direct observations of the atmospheric processing of Asian mineral dust. Atmos. Chem. Phys. 7, 1213–1236. https://doi.org/10.5194/acp-7-1213-2007

Sun, J., Li, Y., Xu, W., Zhou, W., Du, A., Li, L., Du, X., Huang, F., Li, Z., Zhang, Z. (2023). Single-particle volatility and implications for brown carbon absorption in Beijing, China. Sci. Total. Environ. 854, 158874. https://doi.org/10.1016/j.scitotenv.2022.158874

Wang, D., Zhou, B., Fu, Q., Zhao, Q., Zhang, Q., Chen, J., Yang, X., Duan, Y., Li, J. (2016). Intense secondary aerosol formation due to strong atmospheric photochemical reactions in summer: Observations at a rural site in eastern Yangtze River Delta of China. Sci. Total. Environ. 571, 1454–1466. https://doi.org/10.1016/j.scitotenv.2016.06.212

Wang, H., Zhu, B., Zhang, Z., An, J., Shen, L. (2015). Mixing state of individual carbonaceous particles during a severe haze episode in January 2013, Nanjing, China. Particuology 20, 16–23. https://doi.org/10.1016/j.partic.2014.06.013

Wang, H., Wen, J., Xu, J., Tian, Y., Shi, G., Feng, Y., Li, M. (2018). Characteristics of single urban raised dust and soil dust in Tianjin city. Res. Environ. Sci. 31, 844–852. https://doi.org/10.13198/j.issn.1001-6929.2018.02.02 (in Chinese)

Wen, J., Shi, X.R., Tian, Y.Z., Xu, J., Shi, G.L., Feng, Y.C. (2018). Analysis of chemical composition of the fine particulate matter in summer in Tianjin city via a single particle aerosol mass spectrometer (SPAMS). J. Environ. Sci. 39, 3492–3501. https://doi.org/10.13227/j.hjkx.201712102 (in Chinese)

Xu, T., Chen, H., Lu, X., Gross, D.S., Yang, X., Mo, Z., Chen, Z., Liu, H., Mao, J., Liang, G. (2017). Single-particle characterizations of ambient aerosols during a wintertime pollution episode in Nanning: local emissions vs. regional transport. Aerosol Air Qual. Res. 17, 49–58. https://doi.org/10.4209/aaqr.2016.01.0026

Yan, J., Lin, Q., Zhang, M., Zhao, S., Chen, L. (2019). Effect of air masses motion on the rapid change of aerosols in marine atmosphere. J. Environ. Sci. 83, 217–228. https://doi.org/10.1016/j.jes.2019.04.005

Yang, F., Tan, J., Zhao, Q., Du, Z., He, K., Ma, Y., Duan, F., Chen, G. (2011). Characteristics of $PM_{2.5}$ speciation in representative megacities and across China. Atmos. Chem. Phys. 11, 5207–5219. https://doi.org/10.5194/acp-11-5207-2011

Yang, F., Chen, H., Du, J., Yang, X., Gao, S., Chen, J., Geng, F. (2012). Evolution of the mixing state of fine aerosols during haze events in Shanghai. Atmos. Res. 104–105, 193–201. https://doi.org/10.1016/j.atmosres.2011.10.005

Yu, X.-N., Shi, Z., Ma, J., Li, M., Gong, K.J. (2019). Source Apportionment and Mixing State of Single Particles in the Nanjing Jiangbei New Area. J. Environ. Sci. 40, 1521–1528. https://doi.org/10.13227/j.hjkx.201809195 (in Chinese)

Yun, L., Cheng, C., Yang, S., Wang, Z., Li, M., Zhong, Q.E., Mao, L., Liu, S., Cheng, X., Chen, D. (2024). Mixing states and secondary formation processes of organic nitrogen-containing single

particles in Guangzhou, China. J. Environ. Sci. 138, 62–73. https://doi.org/10.1016/j.jes.2023.02.053

Zhai, J., Wang, X., Li, J., Xu, T., Chen, H., Yang, X., Chen, J. (2015). Thermal desorption single particle mass spectrometry of ambient aerosol in Shanghai. Atmos. Environ. 123, 407–414. https://doi.org/10.1016/j.atmosenv.2015.09.001

Zhang, C., Lu, X., Zhai, J., Chen, H., Yang, X., Zhang, Q., Zhao, Q., Fu, Q., Sha, F., Jin, J. (2018). Insights into the formation of secondary organic carbon in the summertime in urban Shanghai. J. Environ. Sci. 72, 118–132. https://doi.org/10.1016/j.jes.2017.12.018

Zhang, G., Bi, X., Li, L., Chan, L., Li, M., Wang, X., Sheng, G., Fu, J., Zhou, Z. (2013). Mixing state of individual submicron carbon-containing particles during spring and fall seasons in urban Guangzhou, China: a case study. Atmos. Chem. Phys. 13, 4723–4735. https://doi.org/10.5194/acp-13-4723-2013

Zhang, G., Han, B., Bi, X., Dai, S., Huang, W., Chen, D., Wang, X., Sheng, G., Fu, J., Zhou, Z. (2015). Characteristics of individual particles in the atmosphere of Guangzhou by single particle mass spectrometry. Atmos. Res. 153, 286–295. https://doi.org/10.1016/j.atmosres.2014.08.016

Zhang, H., Cheng, C., Tao, M. (2017a). Analysis of single particle aerosols in the North China Plain during haze periods. Res. Environ. Sci. 30, 1–9. https://doi.org/10.13198/j.issn.1001-6929.2017.01.41 (in Chinese)

Zhang, J., Luo, B., Zhang, J., Ouyang, F., Song, H., Liu, P., Cao, P., Schäfer, K., Wang, S., Huang, X. (2017b). Analysis of the characteristics of single atmospheric particles in Chengdu using single particle mass spectrometry. Atmos. Environ. 157, 91–100. https://doi.org/10.1016/j.atmosenv.2017.03.012

Zhang, J., Luo, B., Zhang, W., Rao, Z., Song, H. (2019). Single-particle characterization of amine-containing particles during summer and winter in Chengdu. J. Environ. Sci. 39, 3152–3160. https://doi.org/10.19674/j.cnki.issn1000-6923.2019.0372 (in Chinese)

Zhang, Q., Liu, J., Wei, N., Song, C., Peng, J., Wu, L., Mao, H. (2023). Identify the contribution of vehicle non-exhaust emissions: A single particle aerosol mass spectrometer test case at typical road environment. Front. Environ. Sci. Eng. 17, 62. https://doi.org/10.1007/s11783-023-1662-8

Zhou, J., Ren, Y., Hong, G., Lu, N., Li, Z., Li, L., Li, H.l., Jin, W. (2015). Characteristics and formation mechanism of a multi-day haze in the winter of Shijiazhuang using a single particle aerosol mass spectrometer (SPAMS). J. Environ. Sci. 36, 3972–3980. https://doi.org/10.13227/j.hjkx.2015.11.005 (in Chinese)

Zhou, L., Liang, Z., Mabato, B.R.G., Cuevas, R.A.I., Tang, R., Li, M., Cheng, C., Chan, C.K. (2023). Sulfate formation via aerosol-phase SO_2 oxidation by model biomass burning photosensitizers: 3, 4-dimethoxybenzaldehyde, vanillin and syringaldehyde using single-particle mixing-state analysis. Atmos. Chem. Phys. 23, 5251–5261. https://doi.org/10.5194/acp-23-5251-2023

Zhou, Y., Wang, Z., Pei, C., Li, L., Wu, M., Wu, M., Huang, B., Cheng, C., Li, M., Wang, X. (2020). Source-oriented characterization of single particles from in-port ship emissions in Guangzhou, China. Sci. Total. Environ. 724, 138179. https://doi.org/10.1016/j.scitotenv.2020.138179

Zou, J., Xu, F., Zou, B., Li, S., Yang, Z. (2018). Spatial-temporal characteristics of haze in the key tourism cities of China. Trop. Geogr. 38, 143–150. https://doi.org/10.13284/j.cnki.rddl.002999 (in Chinese)